

# RSC Advances



This is an *Accepted Manuscript*, which has been through the Royal Society of Chemistry peer review process and has been accepted for publication.

*Accepted Manuscripts* are published online shortly after acceptance, before technical editing, formatting and proof reading. Using this free service, authors can make their results available to the community, in citable form, before we publish the edited article. This *Accepted Manuscript* will be replaced by the edited, formatted and paginated article as soon as this is available.

You can find more information about *Accepted Manuscripts* in the [Information for Authors](#).

Please note that technical editing may introduce minor changes to the text and/or graphics, which may alter content. The journal's standard [Terms & Conditions](#) and the [Ethical guidelines](#) still apply. In no event shall the Royal Society of Chemistry be held responsible for any errors or omissions in this *Accepted Manuscript* or any consequences arising from the use of any information it contains.

1 **Removal of metformin hydrochloride by *Alternanthera philoxeroides***  
2 **biomass derived porous carbon materials treated with hydrogen**  
3 **peroxide**

4 Xixian Huang<sup>a,b</sup>, Yunguo Liu<sup>a,b,\*</sup>, Shaobo Liu<sup>c,d,\*</sup>, Zhongwu Li<sup>a,b</sup>, Xiaofei Tan<sup>a,b</sup>, Yang  
5 Ding<sup>a,b</sup>, Guangming Zeng<sup>a,b</sup>, Yan Xu<sup>a,b</sup>, Wei Zeng<sup>a,b</sup>, Bohong Zheng<sup>c</sup>

6

7 <sup>a</sup>College of Environmental Science and Engineering, Hunan University, Changsha  
8 410082, PR China.

9 <sup>b</sup>Key Laboratory of Environmental Biology and Pollution Control (Hunan University),  
10 Ministry of Education, Changsha 410082, PR China.

11 <sup>c</sup>School of Architecture and Art Central South University, Central South University,  
12 Changsha 410082, P. R. China.

13 <sup>d</sup>School of Metallurgy and Environmental, Central South University, Changsha 410083,  
14 P.R. China

15

16

---

\* Corresponding author: Tel.: +86 731 88649208; Fax.: +86 731 88822829

E-mail: hnliuyunguo@163.com (Y.G. Liu).

\* Corresponding author: Tel.: +86 731 88830923; Fax.: +86 731 88710171

E-mail: liushaobo23@aliyun.com (S.B. Liu).

17 **Abstract**

18 Hydrogen peroxide modified biochar (mBC) derived from *Alternanthera philoxeroides*  
19 (AP) biomass was used to investigate the adsorption properties of metformin  
20 hydrochloride (MF). Additionally, the effects of pH and Cu (II) on MF adsorption were  
21 also evaluated. Adsorption kinetics and isotherms indicated that the adsorption process  
22 of MF on mBC was fitted better to pseudo-second-order model and Freundlich model,  
23 respectively. The adsorption thermodynamic analysis revealed that the adsorption  
24 processes of MF were spontaneous and endothermic. In this study, there was a great  
25 influence of pH on MF adsorption capacity related to the various species of MF  
26 (cationic, zwitterionic and anionic) at different pH. Furthermore, it could be found that  
27 the presence of Cu (II) facilitated MF adsorption in the range of pH 3.0-7.0, while the  
28 adsorption capacity of MF decreased with the increase of Cu (II) concentration. At pH <  
29 3 or pH > 7, the presence of Cu (II) had only minor effects on MF adsorption.

30

31

32

33

34 Keywords: Biochar; Hydrogen peroxide; Metformin hydrochloride; pH; Cu (II)

35

36

37

## 38 1. Introduction

39 Diabetes Mellitus is threatening more and more people's health, which is a group of  
40 metabolic diseases characterized by hyperglycemia resulting from defects in insulin  
41 secretion, insulin action, or both.<sup>1</sup> Metformin is an antihyperglycemic agent and it can  
42 lower the blood glucose concentration without causing hypoglycemia.<sup>2</sup> However,  
43 metformin has potential harms to humans and animals in natural environment.  
44 Metformin could cause adverse effects on gastrointestinal and lactic acidosis, which is  
45 rare but potentially fatal.<sup>2</sup> The widely prescribed anti-diabetic metformin is among the  
46 most abundant of pharmaceuticals found in effluent and is structurally dissimilar from  
47 hormones.<sup>3</sup> It was reported that a certain concentration of metformin in wastewater  
48 effluent could cause various damages to fathead minnows (*Pimephales promelas*),  
49 including the development of intersex gonads in males, male fish size reduction, and  
50 fecundity reduction. Furthermore, juvenile fathead minnows were more susceptible to  
51 the estrogenic effects of metformin during a 7 day exposure than older and sexually  
52 mature male fathead minnows.<sup>4</sup> Besides, some studies demonstrated that the exposure  
53 of adult fathead minnows (including exposure during the critical period of male sexual  
54 development) to metformin can result in severe endocrine impacts such as intersex.<sup>5,6</sup>  
55 Therefore, metformin acts as an endocrine disruptor at environmentally relevant  
56 concentrations.

57 Recent studies of watersheds downstream of wastewater treatment plants (WWTPs)  
58 showed that anti-diabetic drug metformin is one of the most abundant pharmaceuticals,

59 which was thought to be mostly deposited into the aquatic environment by mass<sup>7</sup> and  
60 detected in effluent at concentrations ranging from 1 to 47  $\mu\text{g L}^{-1}$ .<sup>7,8,9</sup> Although largely  
61 converted to byproducts in WWTPs, the biguanidine drug is excreted in patient's waste  
62 in its active form and is still deposited into the environment in a relatively high amount  
63 for a pharmaceutical, at up to 6 tons per year from individual WWTPs in urban areas.<sup>10</sup>  
64 Thus, it is inevitable to study the adsorption properties of metformin onto adsorbents in  
65 aqueous solutions.

66 Biochar contains porous carbonaceous structure and an array of functional groups,  
67 which is the by-product of biomass pyrolysis under a negligible or limited supply of  
68 oxygen.<sup>11,12</sup> Various types of biomass including wood waste, crop residues, and dairy  
69 manure have been used to produce biochars.<sup>13,14</sup> For instance, biochars derived from  
70 soybean stover and peanut shell had strong affinities for trichloroethylene adsorption.<sup>15</sup>  
71 Similarly, biochar made from agricultural biomass waste exhibited a high adsorption  
72 capacity on organic pollutants.<sup>16</sup> However, the studies of antidiabetic drugs adsorption  
73 by biochar was very scarce, especially metformin hydrochloride.

74 As one of the high-level nutrient adapted hydrophytes, *Alternanthera philoxeroides*  
75 (AP) has been widely used in the ecological restoration of eutrophic lakes.<sup>17</sup> However,  
76 the large amount of AP brings additional problems which need to be handled.<sup>18</sup>  
77 Currently, AP waste is often disposed by natural decomposition, which could cause  
78 secondary environmental problems by releasing pathogens and methane.<sup>18</sup> Therefore,  
79 using AP as a source material for biochar production may be eco-friendly and

80 cost-effective. In addition, the increases of oxygen-containing surface functional groups  
81 and surface area of biochar could enhance the adsorption capacity of pollutants.<sup>15</sup> Thus,  
82 we applied that H<sub>2</sub>O<sub>2</sub>, as a strong oxidant to improve the adsorption performance of  
83 biochar.

84 Recently, the medicinal uses and applications of metals and metal complexes are of  
85 increasing clinical and commercial importance. The metal-drug complexes can be used  
86 to change human abdominal environment. Copper complex is one of the important  
87 metal complexes, which could cause environmental pollution.<sup>19,20</sup> Moreover, metallic  
88 elements play a crucial role in living systems.<sup>21</sup> Metals are easily losing electrons from  
89 the elemental or metallic state to form positively charged ions which tend to be soluble  
90 in biological fluids. Metal ions are electron deficient and most biological molecules are  
91 electron rich. Therefore, these opposing charges attract each other, which may lead to  
92 the general tendency of metal ions to bind to and interact with biological molecules.<sup>20</sup>  
93 Several studies have indicated that the formation of complexes between metallic ions  
94 and organic pollutants would affect the adsorption efficiency of adsorbents. For  
95 example, the presence of metallic ions (Ca<sup>2+</sup>, Mg<sup>2+</sup> and Na<sup>+</sup>) greatly influenced the  
96 sorption of tetracyclines (TC) in soils or mineral constituents, due to the formation of  
97 complexes between metallic ions and TC.<sup>22</sup> Similarly, the coexistence of TC and Cu (II)  
98 could enhance the adsorption of TC on montmorillonite.<sup>23</sup> Furthermore, the complexes  
99 of TC and Cu (II) existed as various species (CuH<sub>2</sub>L<sup>2+</sup>, CuHL<sup>+</sup>, and CuL) at different  
100 solution pH, which had higher adsorption coefficients compared with TC (H<sub>3</sub>L<sup>+</sup>, H<sub>2</sub>L,

101 and  $\text{HL}^-$ ).<sup>24</sup> Thus, heavy metal in the natural environment could affect the transport and  
102 fate of organic pollutants. In addition, the complexation reaction between organic  
103 pollutant and heavy metal at various solution pH values results in different specific  
104 species. Therefore, it is necessary to investigate the effects of pH and the presence of  
105 heavy metal on the adsorption of pollutants on natural sorbents.

106 In this study, AP was used to prepare biochar via slow pyrolysis at 300 °C, and the  
107 resulted biochar was modified by  $\text{H}_2\text{O}_2$ . The modified biochar was applied to determine  
108 the adsorption behavior of MF. To our knowledge, few studies have focused on the  
109 adsorption behavior of MF on biochar, and the effects of pH and Cu (II) on MF  
110 adsorption onto biochar remain unknown. Hence, the specific objectives of this study  
111 were to (1) compare physical and chemical properties of  $\text{H}_2\text{O}_2$ -modified and unmodified  
112 biochar, and the adsorption capacity of MF on  $\text{H}_2\text{O}_2$ -modified and unmodified biochar;  
113 (2) examine isotherms, kinetics and thermodynamic properties of MF sorption onto  
114 mBC; (3) explore the adsorption of MF on mBC as affected by pH and Cu (II).

## 115 **2. Materials and methods**

### 116 **2.1 Biochar preparation**

117 The AP used for biochar production was collected from Changsha, Hunan province,  
118 China. AP was washed with ultrapure water to remove the attached dust, and then dried  
119 at 80 °C for 24 h. Then, the dried biomass were pyrolyzed in a lab-scale tubular reactor  
120 (SK-G08123K, China) at 300 °C and 450 °C, respectively at a heating rate of 5 °C

121  $\text{min}^{-1}$ , in  $\text{N}_2$  environment for 2 h. The biochar samples (BC) were then cooled at room  
122 temperature. BC were ground through a 0.15 mm sieve for this study. The final BC  
123 sample was stored for later experiments.

124 To make the mBC, about 5 g of the final BC sample was placed into 50 mL 15%  
125  $\text{H}_2\text{O}_2$  solution. Then the mixture was ultrasonic dispersion for 2 h. The suspension was  
126 vibrated in oscillator for 5 h at 25 °C, and then rinsed with ultrapure water and dried at  
127 80 °C. The resulted mBC was stored for later experiments.

## 128 **2.2 Biochar characterization**

129 The elemental composition on the sample surface was determined using an ESCALAB  
130 250Xi X-ray Photoelectron Spectrometer (XPS) (Thermo Fisher, USA). Carbon,  
131 hydrogen and nitrogen contents of the samples were determined using a CHN Elemental  
132 Analyzer (Elementar Vario El Cube, Germany). Brunauer, Emmett and Teller (BET)  
133 surface area was determined using a gas sorption analyzer (Quantachrome Quadrasorb  
134 SI, USA) and the total pore volume was examined from the  $\text{N}_2$  adsorption-desorption  
135 isotherms. Fourier transform infra-red spectrophotometer (FTIR) (Nicolet Magna-IR  
136 750, USA) was used to measure the functional groups of sample's surface. The pH of  
137 the point of zero charge ( $\text{pH}_{\text{pzc}}$ ) was measured using Electroacoustic Spectrometer  
138 (ZEN3600 Zetasizer, UK) by adding 0.1 g mBC to solution with pH ranging from 1.0 to  
139 12.0.

## 140 **2.3 Batch adsorption**



141 Ultrapure water with a resistivity of  $18.25 \text{ M}\Omega \text{ cm}^{-1}$  was used in this study. The  
142 concentrations of MF ( $0.05\text{--}3.2 \text{ mmol L}^{-1}$ ) were prepared by dissolving analytic grade  
143 metformin hydrochloride into ultrapure water.

144 The impact of pH on mBC adsorption was examined by adjusting the initial MF  
145 solutions ( $0.5 \text{ mmol L}^{-1}$ ) ranging from 1.0 to 12.0 with 1 M NaOH or 1 M HCl. The  
146 influence of Cu on mBC adsorption was conducted by adding  $\text{Cu}^{2+}$  (0.1, 0.5, and 1  
147  $\text{mmol L}^{-1}$ ) into MF solutions. Adsorption kinetic was conducted by adding 0.1 g mBC  
148 into 50 mL of the  $0.5 \text{ mmol L}^{-1}$  solutions. These suspensions were shaken at 160 rpm at  
149  $25 \text{ }^\circ\text{C}$  for the designated time periods. Experiments for adsorption isotherms were  
150 conducted at the initial concentrations of MF (0.05, 0.1, 0.2, 0.5, 0.8, 1.6, 2.4 and 3.6  
151  $\text{mmol L}^{-1}$ ) and the shaking period of 24 h. Thermodynamic data were obtained at the  
152 temperature of 25, 35 and  $45 \text{ }^\circ\text{C}$  based on the experiments of adsorption isotherms. The  
153 influence of background ionic strength on MF adsorption was determined at appropriate  
154 pH with the addition of different concentrations of NaCl and  $\text{CaCl}_2$  (0, 0.1, 0.2, 0.4, 0.8  
155 and  $1.0 \text{ mmol L}^{-1}$ ). The mBC with 0.1 g was added into each solution, and suspensions  
156 were shaken at 160 rpm under  $25 \text{ }^\circ\text{C}$  for 24 h.

#### 157 **2.4 Desorption experiment**

158 The regeneration study was conducted by using hydrochloric acid as stripping agent.  
159 The mBC which has been used to adsorb MF ( $2.4 \text{ mmol L}^{-1}$ ) was added into 50 mL of  
160  $0.5 \text{ mol L}^{-1}$  HCl solution, shaken at 160 rpm under  $25 \text{ }^\circ\text{C}$  for 10 h. Then the adsorbent

161 was washed to neutral by deionized water and collected to reuse.

## 162 **2.5 MF detection**

163 The concentration of solute in supernatant solution was measured by high performance  
164 liquid chromatography (Agilent 1200, USA) equipped with C18 column with column  
165 temperature at 25 °C. The mobile phase consisted of acetonitrile (65%) and 10 mM  
166 monopotassium phosphate (35%) at a flow rate of 1.0 mL min<sup>-1</sup>. The pH of phosphate  
167 buffer was adjusted to 5.75 with o-phosphoric acid which was filtered through 0.2 µm  
168 filter. MF was analyzed by a UV detector at 233 nm. The calibration curve was linear in  
169 the concentration range of 0.01–0.1 mmol L<sup>-1</sup>.

## 170 **3. Results and discussion**

### 171 **3.1 Characteristics of biochar**

172 The BET characteristics of BC and mBC were presented in Table 1. The BET surface  
173 area of BC increased (from 42.75 to 85.68 m<sup>2</sup> g<sup>-1</sup>) with the increase of pyrolysis  
174 temperature (from 300 to 450 °C). Moreover, the BET surface area of mBC produced at  
175 450 °C was 178.37 m<sup>2</sup> g<sup>-1</sup>, which was higher than that of BC (85.68 m<sup>2</sup> g<sup>-1</sup>). These  
176 results indicated that the surface area of BC increased obviously by increasing pyrolysis  
177 temperature and H<sub>2</sub>O<sub>2</sub> modification.

178 As shown in Table 2, the CHN analysis indicated similar hydrogen and nitrogen  
179 contents of BC and mBC. However, the carbon content of mBC (43.47%) was lower

180 than that of BC (54.93%), suggesting that part of the carbon in BC was oxidized by the  
181  $\text{H}_2\text{O}_2$  resulting in the calculated higher oxygen content of the mBC (49.87%) than that  
182 of BC (36.42%). The surface chemical elements of biochar before and after  
183 modification or adsorption were determined by XPS. The XPS survey spectra (Fig. 1)  
184 indicated that the main elements of mBC made at 300 °C were carbon (75.21%), oxygen  
185 (20.34%) and nitrogen (4.45%), and the contents of these elements changed to 75.57%,  
186 19.36% and 5.07% after MF adsorption, respectively. Moreover, the main elements of  
187 mBC after MF adsorption in the presence of Cu (II) were carbon (75.78%), Oxygen  
188 (18.51%), nitrogen (5.09%), and copper (0.63%). These changes of element content  
189 among three biochars indicated that the presence of MF and/or Cu (II) may influence  
190 the element content, which could be attributed to the adsorption of MF onto biochar. As  
191 shown in Fig. 2, the peaks observed at binding energy of 283.7, 285.4, 286.5 and 287.8  
192 eV for three carbon materials correspond to C–C, C–N, C–O and C=O, respectively. A  
193 new peak of mBC at 288.9 eV could be assigned to  $-\text{COO}-$ .<sup>25</sup> Therefore, these results  
194 indicated that mBC was functionalized well with  $-\text{COO}-$  groups through  $\text{H}_2\text{O}_2$   
195 treatment.

196 The FTIR spectra of BC and mBC produced at 300 °C are shown in Fig. S1.  
197 Characteristic peak at about  $3420\text{ cm}^{-1}$  was related to the stretching vibration of  $-\text{OH}$   
198 groups. The band at  $3155.2\text{ cm}^{-1}$  may be mainly due to the stretching vibration of  $-\text{NH}$   
199 containing in Cu (II)-(MF)<sub>2</sub>.<sup>20</sup> The peak at  $2927.5\text{ cm}^{-1}$  was connected with  
200 asymmetrical stretching vibration of methylene groups and the peak at  $2356.6\text{ cm}^{-1}$

201 could correspond to  $C\equiv C$  in-line deformation vibration or carbon dioxide.<sup>26</sup> The band  
202 near at  $1623.8\text{ cm}^{-1}$  was assigned to the stretching vibration of  $-OH$  deformation of  
203 water and  $C=O$  stretching vibrations of ester.<sup>27</sup> The peak near at  $1430\text{ cm}^{-1}$  may be  
204 attributed to the  $-COO-$  groups and the band near at  $780\text{ cm}^{-1}$  was related to  
205 carboxylate ( $-COO-$ ) deviational vibration and symmetric stretching.<sup>28</sup>

206 The FTIR spectra of BC (Fig. S1a) and mBC (Fig. S1b) revealed that the band at  
207  $1430.9\text{ cm}^{-1}$  shifted to the higher wavenumbers ( $1434.8\text{ cm}^{-1}$ ) after modification, which  
208 demonstrated that  $H_2O_2$  treatment could influence the oxygen-containing functional  
209 groups of biochar surface.<sup>29,30</sup> Compared to the FTIR spectra of mBC (Fig. S1b), the  
210 peak of mBC after MF adsorption (Fig. S1c) at  $1434.8\text{ cm}^{-1}$  and  $782.9\text{ cm}^{-1}$  were shifted  
211 to  $1438.7\text{ cm}^{-1}$  and  $779.1\text{ cm}^{-1}$ , respectively, which may indicate that  $-COO-$  groups on  
212 mBC was contributed to the MF adsorption. In addition, the FTIR spectra of mBC after  
213 MF adsorption in the presence of Cu (II) (Fig. S1d) showed that those peaks, such as  
214  $-CO$ ,  $-OH$ , and  $-COO-$ , had changes compared to other spectrums. The possible  
215 explanation may be that the existence of Cu (II) could influence the adsorption process  
216 of MF on mBC. Moreover, the appearance of the new band at  $3155.2\text{ cm}^{-1}$  may indicate  
217 that a part of MF was adsorbed at the form of  $Cu(II)-(MF)_2$  by mBC.<sup>20</sup>

### 218 3.2 Kinetic studies

219 Pseudo-first-order, pseudo-second-order, and intra-particle diffusion were used to  
220 simulate the kinetic of MF sorption on mBC made at 300 and 450 °C. Governing

221 equations for these models can be written as:<sup>31,32</sup>

222 First-order:  $q_t = q_e(1 - e^{-k_1 t})$  (1)

223 Second-order:  $q_t = \frac{k_2 q_e^2 t}{1 + k_2 q_e t}$  (2)

224 Intra-particle diffusion:  $q_t = k_{pi} t^{1/2} + C$  (3)

225 Where  $q_t$  ( $\mu\text{mol g}^{-1}$ ) and  $q_e$  ( $\mu\text{mol g}^{-1}$ ) are the amount of sorbate removed at time  $t$  and  
226 at equilibrium, respectively, and  $k_1$  ( $\text{min}^{-1}$ ) and  $k_2$  ( $\text{g } \mu\text{mol}^{-1} \text{min}^{-1}$ ) are the first-order and  
227 second order sorption rate constants, respectively. The  $k_{pi}$  ( $\mu\text{mol g}^{-1} \text{min}^{-1/2}$ ) is the  
228 diffusion rate constant of intra-particle.  $C$  is the intercept related to the thickness of the  
229 boundary layer.

230 The relative parameters calculated from pseudo-first-order model,  
231 pseudo-second-order model and intra-particle diffusion model are listed in Table 3. The  
232 correlation coefficient ( $R^2$ ) of the pseudo-second-order model (0.98 and 0.96) was  
233 higher than those of the pseudo-first-order model (0.94 and 0.89), indicating the  
234 experimental data fitted better to pseudo-second-order model. The values of  $q_e$   
235 calculated from pseudo-second-order model (120.81 and 145.65  $\mu\text{mol g}^{-1}$ ) were more  
236 fitted in the experimental value (122 and 153  $\mu\text{mol g}^{-1}$ ). The pseudo-second-order  
237 model supposes that the sorption rate of MF is controlled by chemisorption involving  
238 valence forces through the sharing or exchange of electrons between mBC surface and  
239 MF.<sup>33</sup> Furthermore, as shown in Fig. 3, MF adsorption on mBC at the beginning 8 h was  
240 rapidly and the adsorption capacities were 104 and 132  $\mu\text{mol g}^{-1}$  for mBC pyrolyzed  
241 under 300 °C and 450 °C, respectively.

242 The intra-particle diffusion model indicated that the adsorption process could be  
 243 divided into three steps, including the diffusion of adsorbate through the bulk solution to  
 244 the external surface of biochar, MF pass through the liquid film to the biochar surface,  
 245 and MF interactions with the surface atoms of the biochar.<sup>34</sup> The adsorption rate became  
 246 slower with the adsorption process by comparing the values of  $k_{pi}$ , especially at final  
 247 steps (Table 3). The potential explanations may be attributed to the following factors: (1)  
 248 the enhanced electrostatic repulsion between the mBC surface and the MF; (2) the lower  
 249 driving force resulting from the lower MF concentration; and (3) the smaller pores on  
 250 mBC surface for diffusion.<sup>35,36</sup>

### 251 3.3 Adsorption isotherms

252 Langmuir, Freundlich and Temkin adsorption models were used to fit the MF adsorption  
 253 isotherm data.<sup>37</sup> Governing equations for these models can be written as:

$$254 \text{ Langmuir model: } q_e = \frac{q_{\max} K_L C_e}{1 + K_L C_e} \quad (4)$$

$$255 \text{ Freundlich model: } q_e = K_F C_e^{1/n} \quad (5)$$

$$256 \text{ Temkin model: } q_e = \frac{RT}{b_T} \ln A_T + \frac{RT}{b_T} \ln C_e \quad (6)$$

257 where  $K_L$  and  $K_F$  are the Langmuir bonding term related to interaction energies (L  
 258  $\mu\text{mol}^{-1}$ ) and the Freundlich affinity coefficient ( $(\mu\text{mol g}^{-1}) (\mu\text{mol L}^{-1})^{-n}$ ), respectively.  
 259  $A_T$  is the Tempkin isotherm equilibrium binding constant (L  $\text{g}^{-1}$ ), and  $b_T$  is Tempkin  
 260 isotherm constant.  $R$  is the universal gas constant (8.314 J  $\text{mol}^{-1} \text{K}^{-1}$ ), and  $T$  is absolute  
 261 temperature (K). The  $C_e$  is the equilibrium concentration ( $\mu\text{mol L}^{-1}$ ),  $q_e$  is the amount of

262 MF adsorbed at equilibrium ( $\mu\text{mol g}^{-1}$ ),  $q_{max}$  is the maximum adsorption capacity of the  
263 solute ( $\mu\text{mol g}^{-1}$ ). The  $n$  is the Freundlich linearity constant related to the surface site  
264 heterogeneity. The adsorption represents favorable adsorption condition if  $n$  is greater  
265 than 1 and less than 10 ( $1 < n < 10$ ). The Langmuir model assumes monolayer adsorption  
266 onto a homogeneous surface with no interactions between the adsorbed molecules. The  
267 Freundlich model is an empirical equation commonly used for heterogeneous surfaces.  
268 The Temkin model contains a factor that explicitly taking into account of  
269 adsorbent-adsorbate interactions and its derivation is characterized by a uniform  
270 distribution of binding energies (up to some maximum binding energy).

271 The MF adsorption isotherms on mBC at three temperatures are shown in Fig. 4.  
272 As shown in Table 4, the correlation coefficient ( $R^2$ ) values of Freundlich model (0.99,  
273 0.99, 0.99 and 0.99, 0.99, 0.99) were higher than those of Langmuir model (0.97, 0.96,  
274 0.95 and 0.97, 0.97, 0.96) and Temkin model (0.88, 0.86, 0.85 and 0.85, 0.83, 0.84).  
275 Therefore, these adsorption data of MF onto mBC fitted Freundlich model better than  
276 Langmuir model and Temkin model, indicating that the heterogeneity adsorption of the  
277 MF to the bonding sites could be attributed to the surface functional groups of mBC.<sup>37</sup>  
278 Moreover, the constants  $n$  of Freundlich model at three temperatures were 1.89, 1.99,  
279 2.35 and 1.92, 2.01, 2.27, respectively.

280 Fig. 5 shows the adsorption capacity of MF on BC and mBC at equilibrium. It  
281 demonstrated that the adsorption amount of biochar modified by  $\text{H}_2\text{O}_2$  ( $258 \mu\text{mol g}^{-1}$  for  
282  $300^\circ\text{C}$  and  $335.5 \mu\text{mol g}^{-1}$  for  $450^\circ\text{C}$ ) was higher than that of unmodified biochar ( $226$

283  $\mu\text{mol g}^{-1}$  for 300 °C and 248.5  $\mu\text{mol g}^{-1}$  for 450 °C). The XPS, FTIR and BET studies  
284 indicated that several reasons may be responsible for the increasing adsorption capacity:  
285 (1) mBC was functionalized well with  $-\text{COO}-$  groups comparing with BC, which may  
286 be contributed to the MF adsorption; (2) compared to BC, mBC had a higher surface  
287 area contained more binding sites, which may be related to the MF adsorption; (3) the  
288 surface area increase with the increase of pyrolysis temperature.

### 289 3.4 Adsorption thermodynamic analysis

290 The thermodynamic data, such as Gibbs free energy  $\Delta G^0$ , enthalpy  $\Delta H^0$ , entropy  $\Delta S^0$ ,  
291 can be calculated using the following equations:

$$292 \quad \Delta G^0 = -RT \ln K_e \quad (7)$$

$$293 \quad \ln K_e = \frac{\Delta S^0}{R} - \frac{\Delta H^0}{RT} \quad (8)$$

294 where  $\Delta G^0$  is the stand free energy change of the ion exchange ( $\text{kJ mol}^{-1}$ ),  $\Delta H^0$  ( $\text{kJ}$   
295  $\text{mol}^{-1}$ ) is the enthalpy change,  $\Delta S^0$  ( $\text{J mol}^{-1} \text{K}^{-1}$ ) is the entropy change,  $R$  is the universal  
296 gas constant ( $8.314 \text{ mol}^{-1} \text{K}^{-1}$ ),  $T$  is the absolute temperature (K),  $K_e$  is the  
297 thermodynamic equilibrium constant which was calculated by plotting  $\ln(q_e c_e^{-1})$  versus  
298  $q_e$  and extrapolating to zero  $q_e$ . The values of  $\Delta H^0$  and  $\Delta S^0$  can be determined from the  
299 intercept and slope of the linear plot of  $\Delta G^0$  versus  $T$ .

300 Changes of temperature can affect sorption behavior of organic chemicals on  
301 sorbents. Increasing temperature can enhance the rate of molecular diffusion and  
302 decrease the viscosity of solution. Therefore, it can be easier for sorbate molecules to



303 cross the external boundary layer and move into the internal pores of sorbents.<sup>38</sup>  
304 Thermodynamic parameters calculated by Eqs. (7) – (8) are shown in Table 5. The  
305 maximum adsorption amount of MF was obtained at 45 °C, and the maximum  
306 adsorption capacity ranged from 375  $\mu\text{mol g}^{-1}$  to 435  $\mu\text{mol g}^{-1}$  as the temperature  
307 ranged from 25 °C to 45 °C. The negative values of  $\Delta G^0$  at three temperatures  
308 demonstrated that the process of these adsorption were spontaneous in nature. Moreover,  
309 the more negative  $\Delta G^0$  proved that the driving force of sorption was stronger. The  
310 decrease of  $\Delta G^0$  with increasing temperature indicated that the driving force of sorption  
311 increased due to less occupation of high energy sorption sites. The positive value of  $\Delta H^0$   
312 (7.631  $\text{kJ mol}^{-1}$ ) indicated that it is an endothermic adsorption associated with an  
313 entropy driven process ( $\Delta S^0 > 0$ ). Furthermore, the increasing randomness at the  
314 solution/solid interface during the adsorption was proved by the positive value of  $\Delta S^0$   
315 (33.80  $\text{J mol}^{-1} \text{K}^{-1}$ ). Therefore, the adsorption processes of MF were spontaneous and  
316 endothermic.

### 317 **3.5 Adsorption of MF on biochar as affected by pH and Cu (II)**

318 The pH is a major factor affecting adsorption of ionizable organic contaminants due to  
319 the varied species.<sup>39</sup> MF has positively charged (cationic), zwitterionic, and/or  
320 negatively charged (anionic) species at different pHs due to different  $pK_{a1}$  ( $pK_{a1}=2.97$   
321 and  $pK_{a2}=11.61$ ).<sup>20</sup> The species distribution as function of pH was depicted in Fig. 6. MF  
322 molecules mainly existed as cations at  $\text{pH} < 2.97$  and dominated as anions at  $\text{pH} >$

323 11.61. In the pH range 2.97–11.61, the zwitterion was the most important species. The  
324 zero point of zeta potential ( $\text{pH}_{\text{zpc}}$ ) was 2.6 for mBC (Fig. S2a). When the solution  $\text{pH} <$   
325  $\text{pH}_{\text{zpc}}$ , the mBC surface contained positive charge because of the protonation of mBC's  
326 hydrated surface. Therefore, a strong electrostatic repulsion between positive charged  
327 mBC surface and cationic MF was existed, which could be responsible for the low  
328 adsorption capacity at  $\text{pH} < 3$ . However, mBC became negative charge due to the  
329 deprotonation of adsorbent's hydrated surface when  $\text{pH} > \text{pH}_{\text{zpc}}$ . As shown in Fig. S2b,  
330 the adsorption capacity of MF on mBC increased with the increase of pH values at  $\text{pH} <$   
331 3. At  $\text{pH} > 3$ , the adsorption capacity decreased with the increase of pH values. The  
332 possible explanation may be that the amount of anions would enhance with increasing  
333 pH values at  $\text{pH} > 3$ , so the electrostatic repulsion between the surface of mBC and MF  
334 species (anions) hindered the MF adsorption.

335 In order to evaluate the effects of heavy metals on the adsorption of MF, Cu (II)  
336 (0.1, 0.5, and 1  $\text{mmol L}^{-1}$ ) were added into MF solution at an initial concentration of 0.5  
337  $\text{mmol L}^{-1}$ . The existence of Cu (II) at a low concentration could enhance the adsorption  
338 of MF onto mBC (Fig. S2c). Moreover, a big influence of heavy metals was present at  
339 the pH 3–7, whereas the adsorption of MF in the presence of heavy metal was almost  
340 similar at  $\text{pH} > 7$ . Experiments data indicated that the adsorption capacity of MF  
341 decreased with the increase of Cu (II) concentration when the concentration of Cu (II)  
342 reached up to 0.5 and 1  $\text{mmol L}^{-1}$ .

343 On the one hand, the presence of Cu (II) facilitated MF adsorption on mBC at pH

344 3–7, which may be attributed to the formation of mono and bis-complexes of Cu (II)  
345 and MF ((Cu(MF))<sup>2+</sup> and (Cu(MF)<sub>2</sub>)<sup>2+</sup>), and the reduction of the mobility of MF in  
346 solution<sup>20</sup>. The solubility of (Cu(MF))<sup>2+</sup> and (Cu(MF)<sub>2</sub>)<sup>2+</sup> were lower than those of  
347 cationic, zwitterionic and anionic of MF, showing the increasing hydrophobicity of MF  
348 in the presence of Cu (II).<sup>20,40</sup> The hydrophobic interactions were generally considered  
349 as an important factor for driving organic chemicals sorption on adsorbents. On the  
350 other hand, CuOH<sup>+</sup> and Cu(OH)<sub>2</sub> would form at high pH, which may be contributed to  
351 the minor effects of the presence of Cu (II) on MF adsorption by mBC at pH > 7.<sup>23,41</sup>  
352 Therefore, these results demonstrated that the interactions of Cu (II) and MF at different  
353 solution pH should be taken into account to understand the environmental fate.

### 354 3.6 Effect of background electrolyte on MF removal

355 Fig. 7 showed the effect of background electrolyte on the MF adsorption onto the mBC  
356 at pH 3 in NaCl and CaCl<sub>2</sub> (0, 0.1, 0.2, 0.4, 0.8 and 1.0 mmol L<sup>-1</sup>) solution. As shown in  
357 Fig. 7, the presence of NaCl at low concentration (0.1 mmol L<sup>-1</sup>) had minor effect on  
358 the adsorption capacity of MF. With the increase of NaCl concentration from 0.2 to 1.0  
359 mmol L<sup>-1</sup>, the MF adsorption capacity decreased from 114 to 97 μmol g<sup>-1</sup>. However, the  
360 CaCl<sub>2</sub> could increase MF removal until the concentration of CaCl<sub>2</sub> was 0.2 mmol L<sup>-1</sup>,  
361 and the adsorption capacity increased from 117 to 119 μmol g<sup>-1</sup>. The effect of CaCl<sub>2</sub> on  
362 MF adsorption was sensitive when the concentration of CaCl<sub>2</sub> reached at 0.4 mmol L<sup>-1</sup>.  
363 The possible explanation could be that high concentration of Na<sup>+</sup>, Ca<sup>2+</sup> and Cl<sup>-</sup> can

364 hinder the electrostatic between the charges on biochar surface and MF (cationic) in  
365 solution. Moreover,  $\text{Na}^+$  and  $\text{Ca}^{2+}$  could occupy surface adsorption sites of mBC firstly.  
366 In addition, the high ionic strength of the solution could influence the activity  
367 coefficient of MF, thus decreasing the contact between the sorbent and solute. The study  
368 of the effect of background electrolyte on MF adsorption indicated that electrostatic  
369 force may be one possible sorption mechanism for the removal of MF on mBC.

### 370 **3.7 Regeneration and desorption analysis**

371 Desorption properties of biochar can reflect its practical and economical value. In this  
372 study, the regeneration of mBC was conducted by using  $0.5 \text{ mol L}^{-1}$  hydrochloric acid  
373 desorption. As shown in Fig. 8, the adsorption capacity of MF decreased with the  
374 increase of cycles, but not less than  $198.5 \mu\text{mol g}^{-1}$  in the sixth cycle. Therefore, mBC  
375 can be regenerated by using hydrochloric acid. The reduction of specific surface area,  
376 pore volume and functional groups may contribute to the decreased adsorption capacity  
377 of MF on mBC.

## 378 **4. Conclusions**

379 This study proved that the higher temperature biochar ( $450^\circ\text{C}$ ) and mBC had a higher  
380 adsorption capacity for MF compared to the lower temperature biochar ( $300^\circ\text{C}$ ) and  
381 unmodified biochar.  $\text{H}_2\text{O}_2$  treatment could increase oxygen-containing functional  
382 groups and surface area of biochar. Moreover, the adsorption mechanism was mainly  
383 attributed to the chemisorption. In addition, pH had great influence on MF adsorption

384 by mBC and the optimum pH value was 3. The presence of Cu (II) could influence the  
385 adsorption capacity of MF at pH 3–7, which may be attributed to the formation of  
386 complexes between Cu (II) and MF. However, Cu (II) had minor effects on MF  
387 adsorption capacity at pH > 7.

### 388 **Acknowledgements**

389 This study was financially supported by the National Natural Science Foundation  
390 and Innovation Group of China (Grant no.41271332, 51478470 and 51521006), and the  
391 Hunan Provincial Innovation Foundation For Postgraduate (Grant No. CX2015B090).

### 392 **References**

- 393 1. A. D. Association, *Diabetes. Care.*, 2010, 33, S62–S69.
- 394 2. T. Klepser, M. Kelly, *Am. J. Health-Syst. Ph.*, 1997, 54, 893–903.
- 395 3. N. J. Niemuth, R. D. Klaper, *Chemosphere*, 2015a, 135, 38–45.
- 396 4. J. Crago, C. Bui, S. Grewal, D. Schlenk, *Gen. Comp. Endocr.*, 2016, In press.
- 397 5. R. Van Aerle, T. J. Runnalls, C. R. Tyler, *J. Fish Biol.*, 2004, 64, 335–369.
- 398 6. N. J. Niemuth, R. Jordan, J. Crago, C. Blanksma, R. Johnson, R. D. Klaper, *Environ.*  
399 *Toxicol. Chem.*, 2015b, 34, 291–296.
- 400 7. M. Oosterhuis, F. Sacher, T. L. Ter Laak, *Sci. Total. Environ.*, 2013, 442, 380–388.
- 401 8. M. Scheurer, A. Michel, H. J. Brauch, W. Ruck, F. Sacher, *Water. Res.*, 2012, 46,  
402 4790–4802.
- 403 9. A. J. Ghoshdastidar, S. Fox, A.Z. Tong, *Environ. Sci. Pollut. Res. Int.*, 2014, 22,

- 404 689–700.
- 405 10. B. D. Blair, J. P. Crago, C. J. Hedman, R. J. F. Treguer, C. Magruder, L. S. Royer, R.  
406 D. Klaper, *Sci. Total. Environ.*, 2013b, 444, 515–521.
- 407 11. X. Tan, Y. Liu, Y. Gu, Y. Xu, G. Zeng, X. Hu, S. Liu, X. Wang, S. Liu, J. Li,  
408 *Bioresour. Technol.*, 2016, 212, 318–333.
- 409 12. X. Tan, Y. Liu, G. Zeng, X. Wang, X. Hu, Y. Gu, Z. Yang, *Chemosphere*, 2015,  
410 125, 70–85.
- 411 13. X. Chen, G. Chen, L. Chen, Y. Chen, J. Lehmann, M. B. McBride, A. G. Hay,  
412 *Bioresour. Technol.*, 2011, 102, 8877–8884.
- 413 14. W. K. Kim, T. Shim, Y. S. Kim, S. Hyun, C. Ryu, Y. K. Park, J. Jung, *Bioresour.*  
414 *Technol.*, 2013, 138, 266–270.
- 415 15. M. Ahmad, S. S. Lee, X. Dou, D. Mohan, J. K. Sung, J. E. Yang, Y. S. Ok,  
416 *Bioresour. Technol.*, 2012, 118, 536–544.
- 417 16. B. Chen, Z. Chen, S. Lv, *Bioresour. Technol.*, 2011, 102, 716–723.
- 418 17. B. Qin, *Ecol. Eng.*, 2009, 35, 1569–1573.
- 419 18. L. Xiao, L. Ynag, Y. Zhang, Y. Gu, L. Jiang, B. Qin, *Ecol. Eng.*, 2009, 35,  
420 1668–1676.
- 421 19. M. M. Correia dos Santos, V. Famila, M. L. Simoes Goncalves, *Anal. Biochem.*,  
422 2002, 303, 111–119.
- 423 20. S. R. Devi, *Int. J. Eng. Sci. Invent.*, 2013, 2, 39–50.
- 424 21. G. Wilkinsion, R. D. Gillard, J. A. McCleverty, *Pergamen, Oxford*, 1987.

- 425 22. T. X. Bui, H. Choi, *Chemosphere*, 2010, 80, 681–686.
- 426 23. Y. J. Wang, D. A. Jia, R. J. Sun, H. W. Zhu, D. M. Zhou, *Environ. Sci. Technol.*,  
427 2008, 42, 3254–3259.
- 428 24. Z. Zhang, K. Sun, B. Gao, G. Zhang, X. Liu, Y. Zhao, *J. Hazard. Mater.*, 2011, 190,  
429 856–862.
- 430 25. S. Stankovich, D. A. Dikin, R. D. Piner, K. A. Kohlhaas, A. Kleinhammes, Y. Jia,  
431 Y., Wu, S. T. Nguyen, R. S. Ruoff, *Carbon*, 2007, 45, 1558–1565.
- 432 26. L. Tang, G. D. Yang, G. M. Zeng, Y. Cai, S. S. Li, Y. Y. Zhou, Y. Pang, Y. Y. Liu,  
433 Y. Zhang, B. Luna, *Chem. Eng. J.*, 2014, 239, 114–122.
- 434 27. D. D. Das, M. I. Schnitzer, C. M. Monreal, P. Mayer, *Bioresour. Technol.*, 2009,  
435 100, 6524–6532.
- 436 28. T. Y. Jiang, J. Jiang, R. K. Xu, Z. Li, *Chemosphere*, 2012, 89, 249–256.
- 437 29. C. Moreno-Castilla, M. A. Ferro-Garcia, J. P. Joly, I. Bautista-Toledo, F.  
438 Carrasco-Marin, J. Rivera-Utrilla, *Langmuir*, 1995, 11, 4386–4392.
- 439 30. M. B. Ahmed, J. L. Zhou, H. H. Ngo, W. Guo, M. Chen, *Bioresour. Technol.*, 2016,  
440 214, 836–851.
- 441 31. Y. S. Ho, G. McKay, *Process. Biochem.*, 1999, 34, 451–465.
- 442 32. Y. Sun, Q. Yue, B. Gao, Y. Gao, X. Xu, Q. Li, Y. Wang, *J. Taiwan. Inst. Chem. E.*,  
443 2014, 45, 681–688.
- 444 33. J. Febrianto, A. N. Kosasih, J. Sunarso, Y. H. Ju, N. Indraswati, S. Ismadji, *J.*  
445 *Hazard. Mater.*, 2009, 162, 616–45.

- 446 34. S. Sen Gupta, K. G. Bhattacharyya, *Adv. Colloid. Interface.*, 2011, 162, 39–58.
- 447 35. W. Liu, J. Zhang, C. Zhang, L. Ren, *Chem. Eng. J.*, 2011, 171, 431–438.
- 448 36. M. J. Ahmed, S. K. Theydan, *Powder. Technol.*, 2012, 229, 237–45.
- 449 37. K. Foo, B. Hameed, *Chem. Eng. J.*, 2010, 156, 2–10.
- 450 38. Z. Y. Wang, X.D. Yu, B. Pan, B.S. Xing, *Environ. Sci. Technol.*, 2010, 44,
- 451 978–984.
- 452 39. D. Zhang, B. Pan, H. Zhang, P. Ning, B. S. Xing, *Environ. Sci. Technol.*, 2010, 44,
- 453 3805–3811.
- 454 40. H. Li, D. Zhang, X. Han, B. Xing, *Chemosphere*, 2014, 95, 150–155.
- 455 41. D. A. Jia, D. M. Zhou, Y. J. Wang, H. W. Zhu, J. L. Chen, *Geoderma*, 2008, 146,
- 456 224–230.



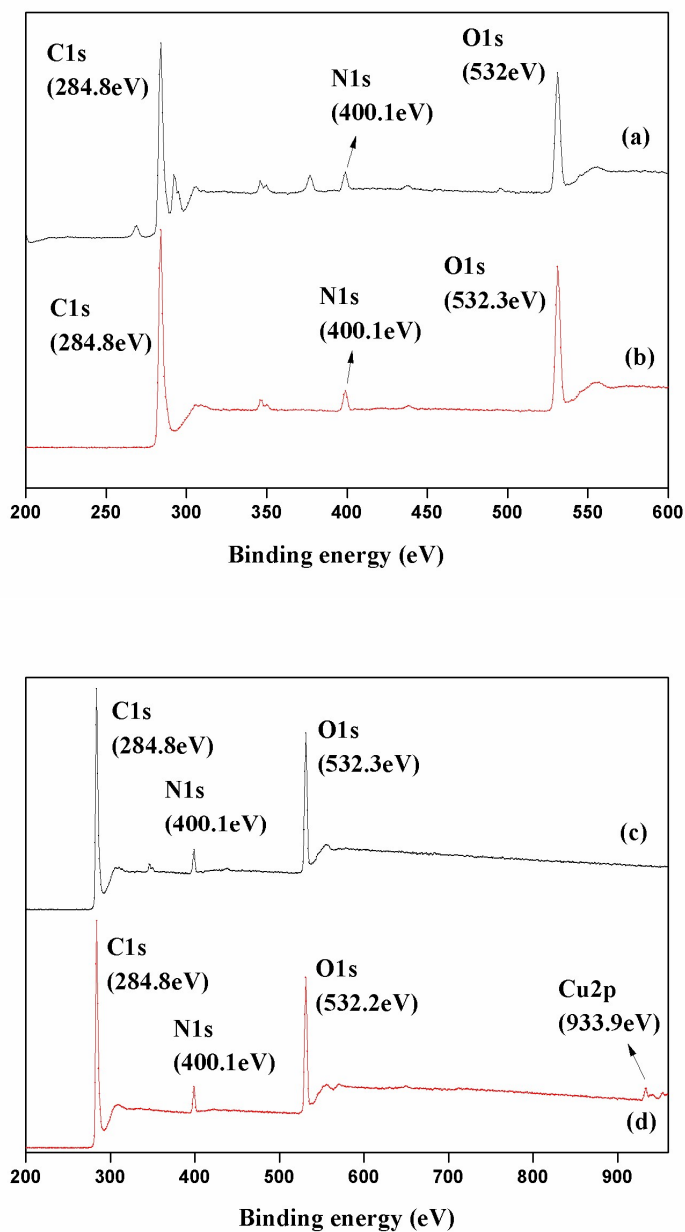


**Fig. 1.** XPS survey spectra of (a) pristine biochar (BC), (b) H<sub>2</sub>O<sub>2</sub>-modified biochar (mBC), (c) metformin hydrochloride (MF) adsorption on mBC, and (d) MF and Cu (II) adsorption on mBC (biochar: 300 °C).

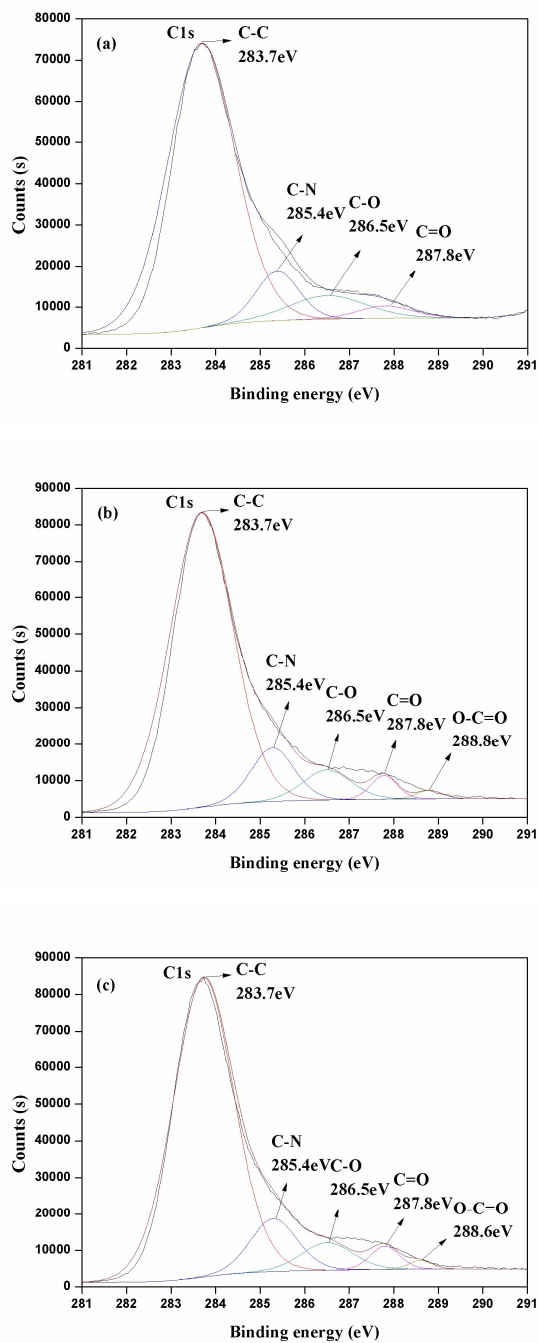


**Fig. 2.** C 1s XPS spectra of (a) Pristine biochar (BC), (b) H<sub>2</sub>O<sub>2</sub>-modified biochar (mBC), and (c) mBC after metformin hydrochloride (MF) adsorption (biochar: 300 °C).

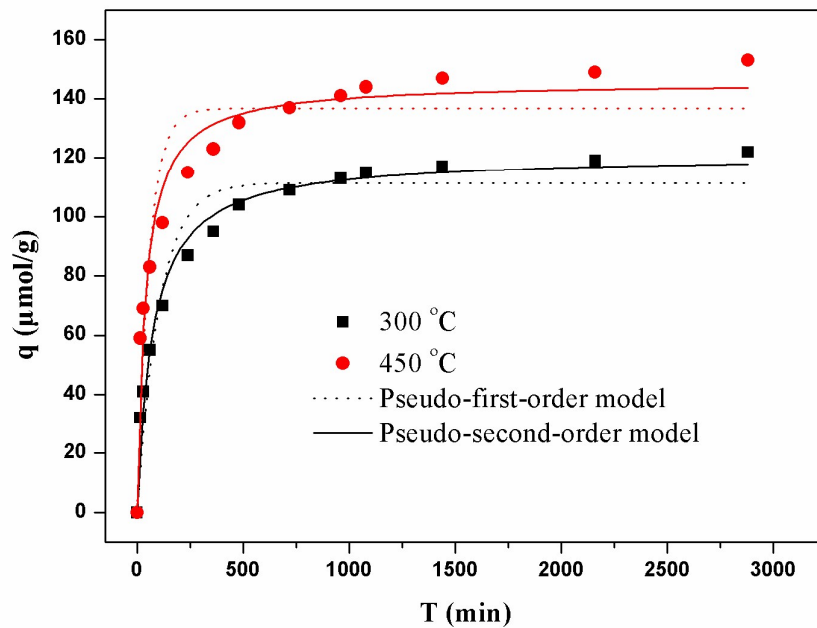


**Fig. 3.** Pseudo-first-order sorption kinetics and pseudo-second-order sorption kinetics for MF adsorption onto mBC (initial MF concentration:  $0.5 \text{ mmol L}^{-1}$ ; pH: 3.0; reaction temperature:  $25 \text{ }^\circ\text{C}$ ).

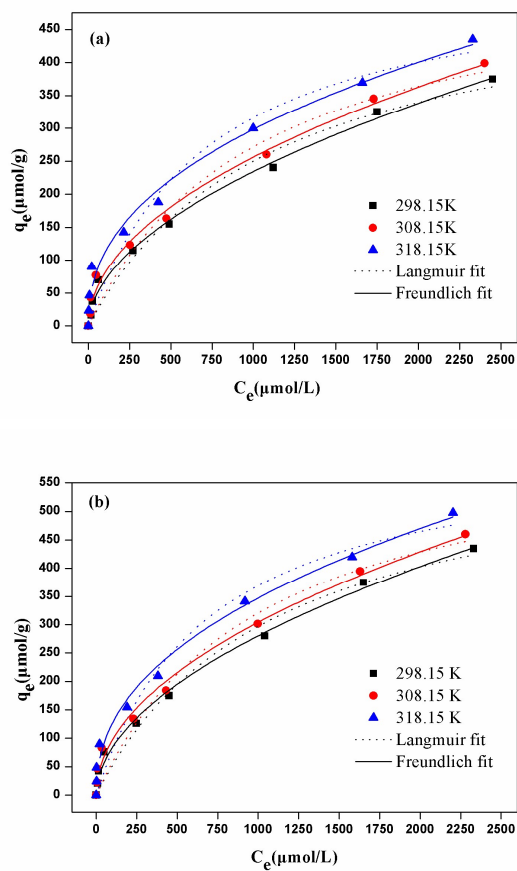


**Fig. 4.** Langmuir isotherm and freundlich isotherm for the adsorption of MF on (a) 300 °C and (b) 450 °C mBC (solution volume: 50 mL; adsorbent dose: 0.1 g; contact time: 24 h; pH: 3.0).

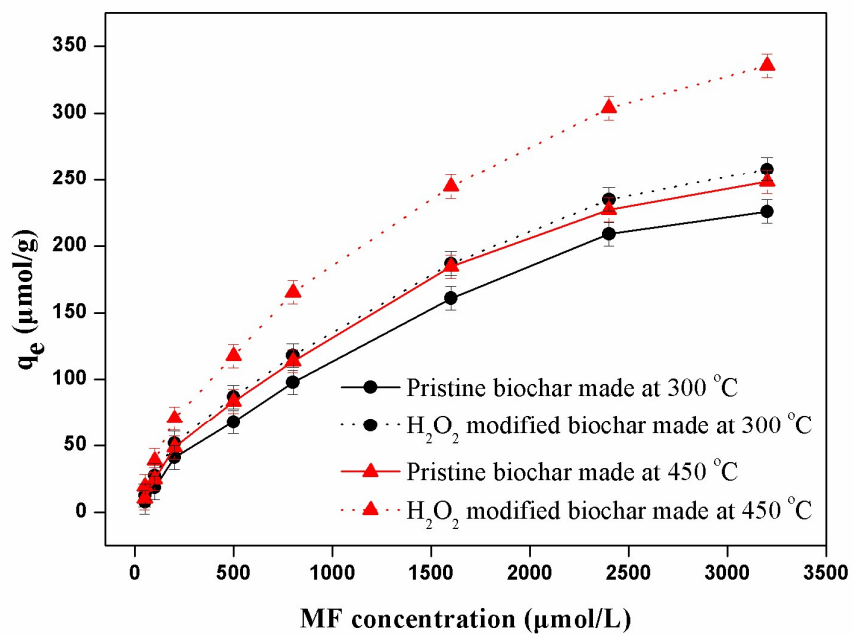


**Fig. 5.** The adsorption capacity of MF on BC and mBC at equilibrium (solution volume: 50 mL; adsorbent dose: 0.1 g; contact time: 24 h; pH: 7.0).

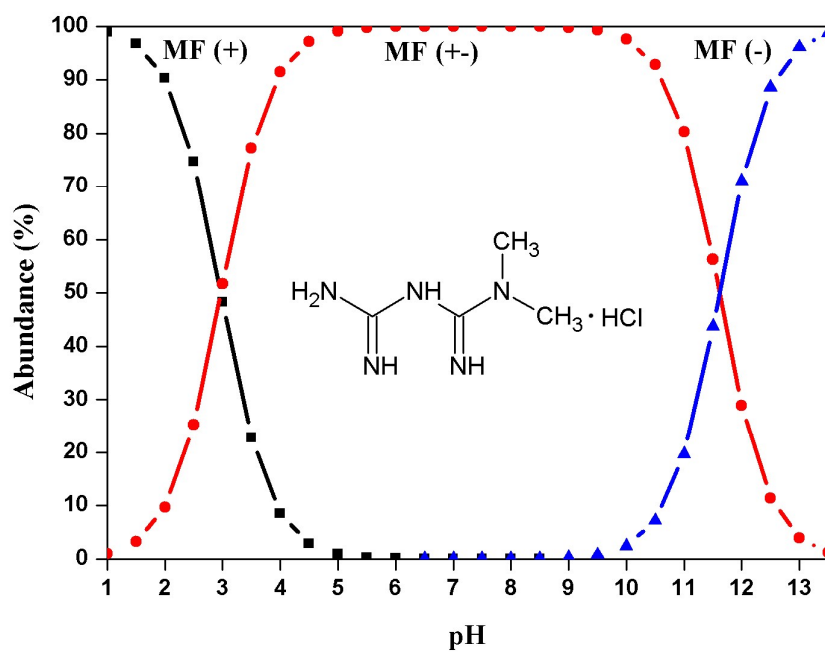
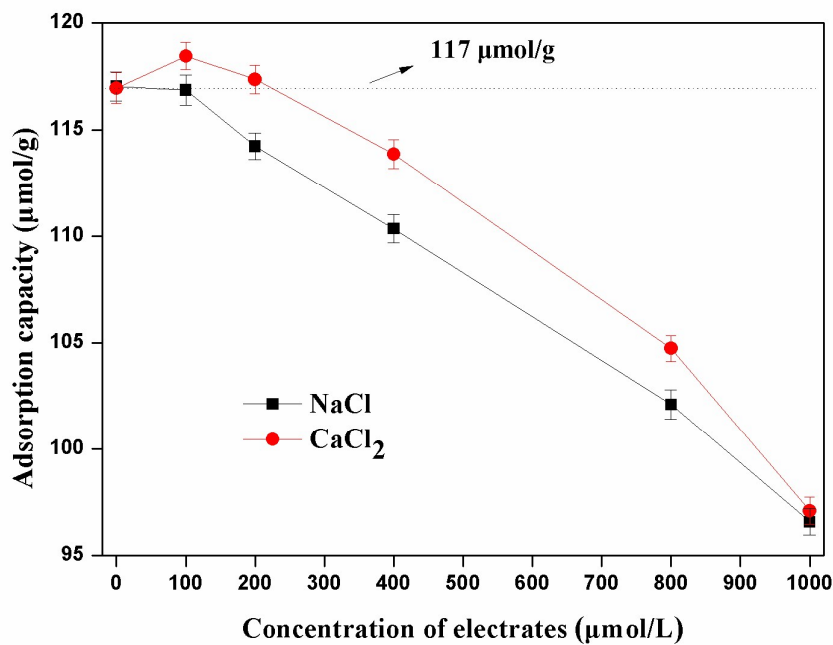
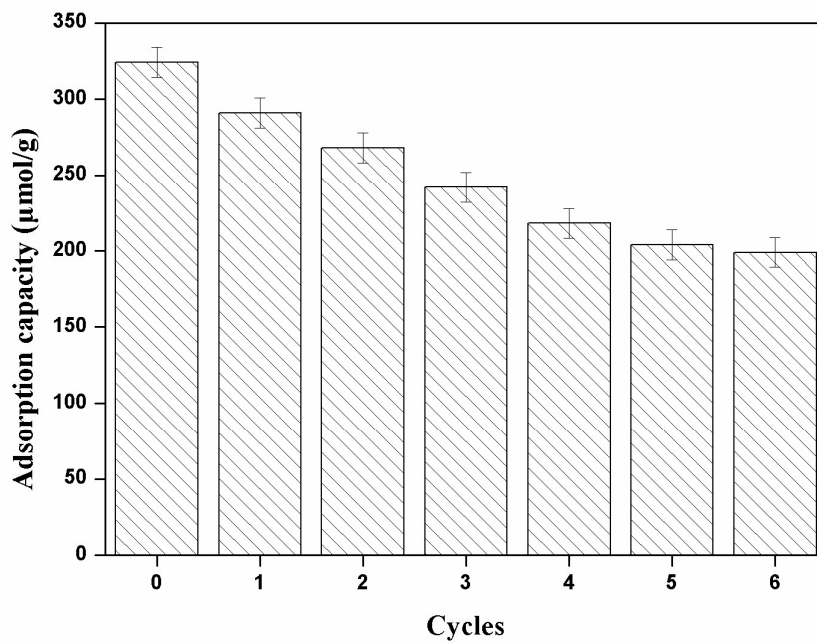


Fig. 6. Molecular structure and speciation of MF under different pH conditions.



**Fig. 7.** Effect of background electrolyte (NaCl and CaCl<sub>2</sub>) on the MF adsorption by mBC. The line of dashes indicating the adsorption capacity of MF without any interfering electrolytes (MF concentration: 0.5 mmol L<sup>-1</sup>; solution volume: 50 mL; adsorbent dose: 0.1 g; contact time: 24 h; temperature: 25 °C; pH: 3.0; biochar: 300 °C).



**Fig. 8.** Adsorption and desorption cycles of mBC for MF adsorption. (MF concentration:  $2.4 \text{ mmol L}^{-1}$ ; solution volume: 50 mL; adsorbent dose: 0.1 g; contact time: 24 h; temperature:  $25 \text{ }^{\circ}\text{C}$ ; pH: 3.0; biochar:  $300 \text{ }^{\circ}\text{C}$ ).



**Table 1 BET characteristics of biochar (BC) and H<sub>2</sub>O<sub>2</sub>-modified biochar (mBC) produced from AP.**

Adsorbent	Pyrolysis temperature (°C)	BET surface area (m <sup>2</sup> g <sup>-1</sup> )	Pore volume (cm <sup>3</sup> g <sup>-1</sup> )	Average pore (nm)
Biochar	300	42.75	0.05786	4.962
	450	85.68	0.07358	5.384
H <sub>2</sub> O <sub>2</sub> -modified biochar	300	114.91	0.09962	5.867
	450	178.37	0.13240	5.952

**Table 2 Bulk elemental composition of biochars made at 300 °C.**

	C(%)	H(%)	O <sup>a</sup> (%)	N(%)	H/C	O/C	N/C
BC	54.93	4.66	36.42	3.99	1.02	0.50	0.06
mBC	43.47	3.66	49.78	3.09	1.01	0.86	0.06

<sup>a</sup> Determined by weight difference assuming that the total weight of the samples was made up of the tested elements only.

**Table 3 Pseudo-first-order and pseudo-second-order model parameters for metformin hydrochloride (MF) sorption on H<sub>2</sub>O<sub>2</sub>-modified biochar (mBC) (300 °C) at 25 °C.**

Kinetic models	Parameters		
	Units	300 °C	450 °C
Pseudo-first-order parameters	$K_1$ (min <sup>-1</sup> )	$9.57 \times 10^{-3}$	$1.77 \times 10^{-2}$
	$q_e$ (μmol g <sup>-1</sup> )	111.44	136.77
	$R^2$	0.94	0.89
Pseudo-second-order parameters	$K_2$ (g μmol <sup>-1</sup> min <sup>-1</sup> )	$1.14 \times 10^{-4}$	$1.76 \times 10^{-4}$
	$q_e$ (μmol g <sup>-1</sup> )	120.81	145.65
	$R^2$	0.98	0.96
Intra-particle diffusion parameters	$k_{p1}$ (μmol g <sup>-1</sup> min <sup>-1/2</sup> )	6.37	5.52
	$C_1$	3.89	38.57
	$R_1^2$	0.97	0.98
	$k_{p2}$ (μmol g <sup>-1</sup> min <sup>-1/2</sup> )	1.66	1.98
	$C_2$	63.61	85.57
	$R_2^2$	0.92	0.93
	$k_{p3}$ (μmol g <sup>-1</sup> min <sup>-1/2</sup> )	0.32	0.36
	$C_3$	104.47	132.91
$R_3^2$	0.98	0.97	

**Table 4 Langmuir, Freundlich and Temkin isotherms parameters for MF sorption on mBC produced at 300 °C.**

Biochar (°C)	Temperature (K)	Langmuir model			Freundlich model			Temkin model		
		$q_{\max}$ ( $\mu\text{mol g}^{-1}$ )	$K_L$ ( $\text{L } \mu\text{mol}^{-1}$ )	$R^2$	$K_F$ ( $\text{L } \mu\text{mol}^{-1}$ )	$n$	$R^2$	$A_T$ ( $\text{L g}^{-1}$ )	$b_T$	$R^2$
300	298.15	528.10	$8.99 \times 10^{-4}$	0.97	6.03	1.89	0.99	0.05062	37.84	0.88
	308.15	551.36	$9.71 \times 10^{-4}$	0.96	8.01	1.99	0.99	0.02181	40.94	0.86
	318.15	546.10	$1.37 \times 10^{-3}$	0.95	15.77	2.35	0.99	0.2126	47.81	0.85
450	298.15	625.27	$9.03 \times 10^{-4}$	0.97	7.50	1.92	0.99	0.08291	36.59	0.85
	308.15	648.05	$9.78 \times 10^{-4}$	0.97	9.87	2.01	0.99	0.1620	41.06	0.83
	318.15	627.12	$1.43 \times 10^{-3}$	0.96	16.93	2.27	0.99	0.3867	44.92	0.84

**Table 5 Thermodynamic parameters for the adsorption of MF by mBC produced at 300 °C.**

$\ln k_e$			$\Delta G^0$ (kJ mol <sup>-1</sup> )			$\Delta H^0$ (kJ mol <sup>-1</sup> )	$\Delta S^0$ (J mol <sup>-1</sup> K <sup>-1</sup> )
298.15 K	308.15 K	318.15 K	298.15 K	308.15 K	318.15 K		
0.9858	1.089	1.176	-2.444	-2.789	-3.120	7.631	33.80